Spontaneously periodic wave generation in coupled excitable media

Lei Zhang,[1] Shengli Zhang,[1,2,*] Huimin Tong,[1] Dongsheng Lei,[1] and Bambi Hu[2,3]
[1]*Department of Applied Physics, Xi'an Jiaotong University, Xi'an 710049, China*
[2]*Department of Physics, Centre for Nonlinear Studies, and The Beijing-Hong Kong-Singapore Joint Centre for Nonlinear and Complex Systems (Hong Kong), Hong Kong Baptist University, Kowloon Tong, Hong Kong, China*
[3]*Department of Physics, University of Houston, Houston, Texas 77204-5005, USA*
(Received 31 October 2007; revised manuscript received 28 January 2009; published 13 May 2009)

We studied a modified reaction-diffusion model theoretically by coupling two ideal excitable media systems. In the simulated homogeneous system, we observed the propagation of reaction-diffusion wave trains that required no external force after the initial stimulation. We investigated the dependence of the system's oscillation patterns on model parameters, and we discussed the influence of the different dynamic constants of the individual coupled systems on the dynamics of the coupled systems. Some complex two-dimensional patterns generated by our model are shown. We also found similar phenomena in the models for catalytic CO oxidation on Pt(110), and for cardiac tissue.

DOI: 10.1103/PhysRevE.79.056213 PACS number(s): 89.75.Kd, 82.40.Ck, 05.65.+b, 47.54.−r

I. INTRODUCTION

Pattern formation and wave evolution have attracted a great deal of attention in physics, chemistry, and biology because they are important to understanding the morphogenesis and other functional aspects of soft condensed-matter systems [1]. Excitable media systems are typically chemical systems that generate spirals and pulses [2], and are used to model the Belousov-Zhabotinsky reaction [3–6], the aggregation of slime molds [7], and the behaviors of the heart muscle [8] and cardiac tissue [9]. To further understand these systems, their pattern formations have been studied in response to external forcing [10–17], and to local [18], nonlocal [19], and global [20] feedback mechanisms.

All complex systems in nature are composites of many simple subsystems, and thorough research into these simple systems can lead to an understanding of the larger ones. These subsystems are rarely independent—on the contrary, they interact with each other. The coupling of several ideal systems may create new characteristics. The importance of this coupling effect, then, should be considered. For example, if there are two predator-prey systems in which the two predators also prey on each other, interesting population dynamics may appear.

Recently, coupled nonlinear systems have been widely studied, theoretically and experimentally. In coupled excitable media systems, for example, Hildebrand *et al.* [21] experimentally and theoretically investigated two locally coupled domains of Belousov-Zhabotinsky systems, and observed beautiful traveling-wave patterns. Li and Lang [22] studied the spatiotemporal dynamics of a one-way coupled FitzHugh-Nagumo system and showed the effects of the coupling effect. Karnatak *et al.* [23] studied identical coupled oscillators and observed amplitude death phenomena.

In this paper, we couple two reaction-diffusion systems in homogeneous excitable media, and we find that periodic wave patterns need no external influence after the initial stimulation. We also investigate the coupling effect in the models for catalytic CO oxidation on Pt(110), and in models for cardiac tissue, and find similar periodic patterns in these two models.

This paper is organized as follows: The coupled model is proposed and simulated in Sec. II. The observation results for the catalytic CO oxidation on Pt(110) and the cardiac tissue models are described in Sec. III. Finally, conclusions and discussions are given in Sec. IV.

II. COUPLED MODEL

A. Model equations

We adopted the simple ideal model as which was used by Barkley [2]. The two activator variables, u_1, u_2, and the two inhibitor variables, v_1, v_2, in our model obey the following equations:

$$\frac{\partial u_1}{\partial t} = \frac{1}{\varepsilon_1} u_1(1-u_1)[u_1 - (v_1+b_1)/a_1] + D_1\nabla^2 u_1, \quad (1)$$

$$\frac{\partial v_1}{\partial t} = u_1 - v_1 - K v_1 v_2, \quad (2)$$

$$\frac{\partial u_2}{\partial t} = \frac{1}{\varepsilon_2} u_2(1-u_2)[u_2 - (v_2+b_2)/a_2] + D_2\nabla^2 u_2, \quad (3)$$

$$\frac{\partial v_2}{\partial t} = u_2 - v_2 - K v_1 v_2. \quad (4)$$

All the parameters and constants are dimensionless. The constants $\varepsilon_{1,2}$ are the ratio of the characteristic time scales of the activator and inhibitor variables; $D_{1,2}$ are diffusion constants; and $a_{1,2}$ and $b_{1,2}$ represent, respectively, the slope of the $u_{1,2}$ nullcline and the excitation threshold. These two systems are coupled through the inhibitor variables v_1 and v_2 with the coupling constant K.

*zhangsl@mail.xjtu.edu.cn

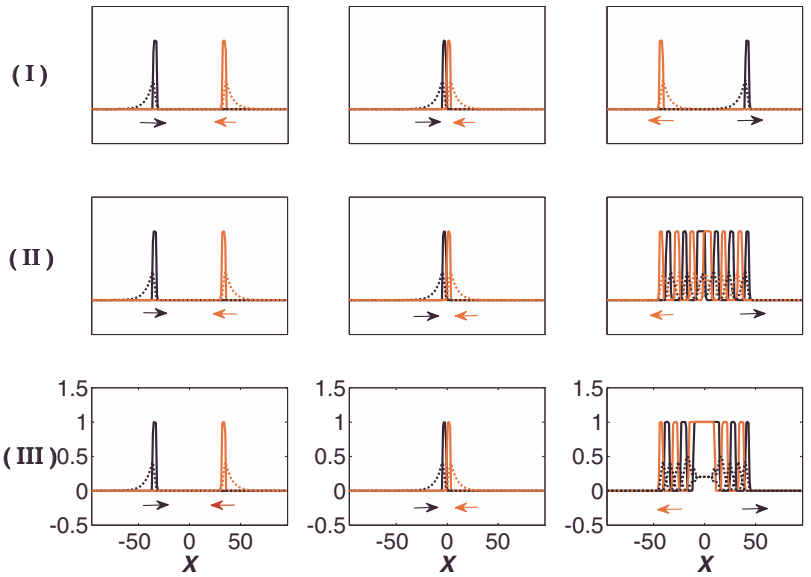

FIG. 1. (Color online) Collision of two single pulses for (I) $K=0$, (II) $K=10$, (III) $K=20$. Time is $t=0$, 6, and 12 from left to right. Parameters are $a=0.4$, $b=0.003$, $\varepsilon=0.0085$, and $D=1$. Unless otherwise indicated, all the following figures use these same parameter values as this figure, and all the parameters are dimensionless.

B. Patterns observed in the model by one-dimensional simulation

To investigate the systems' spatiotemporal dynamics, the parameters K, $a_{1,2}$, and $b_{1,2}$ were varied. We used the explicit Euler method with a five-point [for two-dimensional (2D)] or three-point [for one-dimensional (1D)] Laplacian and no-flux boundary conditions for our numerical calculations. Throughout the following simulations a time step of 0.001 and a space step of 1 were used.

Obviously, if $K=0$, the whole system reduces to two independent systems, both of which obey the standard reaction-diffusion model as discussed in Ref. [2]. For $K>0$, in the case of the head-on collision of the $u_{1,2}$ and $v_{1,2}$ pulses, the two inhibitor variables, v_1 and v_2, begin to interact, and they decrease within the regions where they are in contact. Unlike the case of single-pulse generation in the single reaction-diffusion system [2], some interesting phenomena consequently appear in these contact regions. At first, for simplicity, we set $a_1=a_2=a=0.4$, $b_1=b_2=b=0.003$, $\varepsilon_1=\varepsilon_2=\varepsilon=0.0085$, and $D_1=D_2=D=1$.

Figures 1–4 show the one-dimensional solution (where $\nabla^2=d^2/dX^2$) of Eqs. (1)–(4). Initially, the four variables were set to zero except u_1 near the left extremity and u_2 near the right extremity (the initial stimulation). The two pulses of u_1 and u_2, which are followed by two v_1 and v_2 pulses, then move toward each other and make contact in the region around $X=0$ (we call this region the contacting region).

Typically, three different spatiotemporal patterns (indicated by I, II, and III in Figs. 1 and 2) are observed with different K values. For very small K values, the u_1 pulse and u_2 pulse simply cross each other [Fig. 1(I) and Fig. 2(I)]. For larger K values, a pulse generator appears in the contacting region and produces stable wave trains where the pulses collide [Fig. 1(II) and Fig. 2(II)]. For pattern III, where K values are much larger, the contacting region also becomes a pulse generator. Now, however, the pulse generator region expands

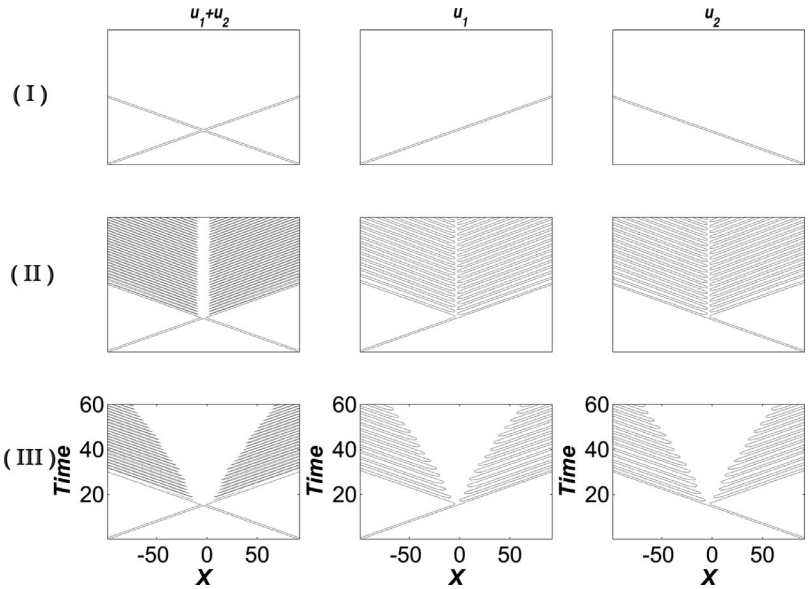

FIG. 2. Spatiotemporal patterns caused by the collisions for (I) $K=0$, (II) $K=10$, and (III) $K=20$. From left to right are the patterns of u_1+u_2, u_1, and u_2. The lines indicate the contour lines of $u_1+u_2=0.1$, $u_1=0.1$, and $u_2=0.1$, respectively.

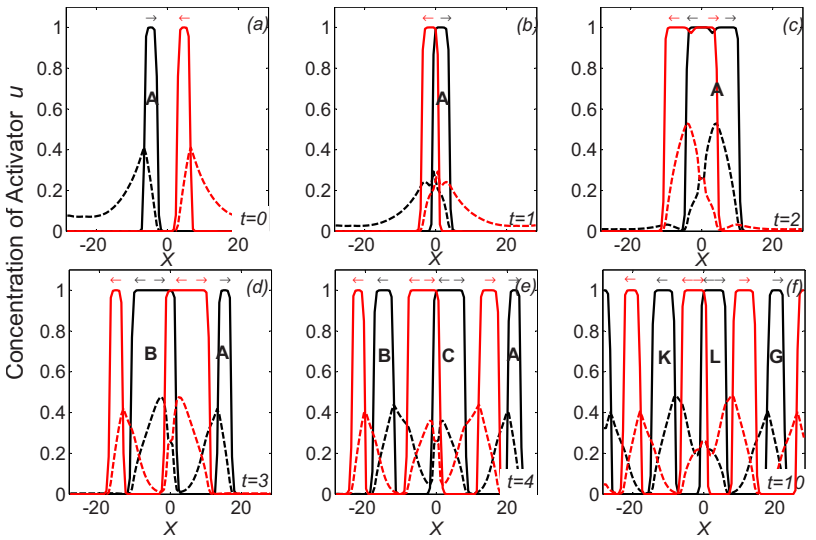

FIG. 3. (Color online) The distribution of u_1 (solid black line), u_2 (solid red line), v_1 (black dashed line), and v_2 (red dashed line) at different times. The black and red arrows above the curve show the direction of motion of the u_1 and u_2 waves.

[Fig. 1(III) and Fig. 2(III), unlike in pattern II whose pulse generator region is localized].

We show the process of the formation of pattern II in Fig. 3. After the two initial pulses of u_1 (labeled A in Fig. 3) and u_2 move toward each other, they make contact in the region around $X=0$ [Figs. 3(a) and 3(b)]. Because v_1 and v_2 will interact in this contacting region [$X=0$; see the black and red dashed lines in Figs. 3(b) and 3(c) for details], the concentration of $v_{1,2}$ begins to decrease. In this case, u_1 and u_2 are not inhibited. They regrow in the contacting region [see Fig. 3(c)]. The left part of pulse A regrows because the concentration of v_1 in this region is decreased by v_2. Consequently, pulse A is split into two pulses at the point where v_1 reaches a certain high value (that is, when $v_1 > a-b$, to be discussed in the next subsection). The new u_1 pulse B appears, and moves toward the left. When pulse B passes the contacting region, its right portion regrows and forms a new pulse C, which moves toward the right. There is always a u_1 pulse that moves back and forth in the contacting region, and continually emits pulses. The whole system stays in the stable state as the pulses fill the system throughout [Fig. 1(II) and Fig. 2(II)], as in Refs. [24,25].

The temporal periodicity (after a short period of adaptation in which the system reaches the stable state, shown in the inset of Fig. 6) of three space points in our model is shown in Fig. 4(a). The solid red, blue dashed, and solid black lines represent the temporal behavior of points $X=18$, $X=-18$, and $X=0$, respectively, where $t=0$ is the point at which the systems reach the stable state. The concentration of u_1 at these space points undergoes periodic oscillations, while at the point $X=0$ it fluctuates very little—its value is always above 0.9 [indicated by the black line around $u_1(X)=1$ in Fig. 4(a)]. In Fig. 4(b) we show the u_1-v_1 cycle orbit at point $X=-18$, which follows the dynamics described by the standard reaction-diffusion model in Ref. [2]. [As described in detail in Ref. [2], while u, v stay at the state of ($u=0$, $v=0$) at first, if u has a perturbation larger than b/a, u will rapidly increase to the maximum value 1, as ε is very small. Then, v will increase as $u-v>0$. When v is larger than $(a-b)$, which makes $1-(v+b)/a<0$, u will rapidly decrease back to 0 and, consequently, v will decrease to 0 exponentially.] In contrast to the standard model, Fig. 4(c) shows that the u_1-v_1 relationship at the point $X=0$ is different. The coupled system stays near a fixed point ($u_1 \approx 1, v_1 \approx 0.27$), indicating that this coupled system reaches a different stable state at the contacting region.

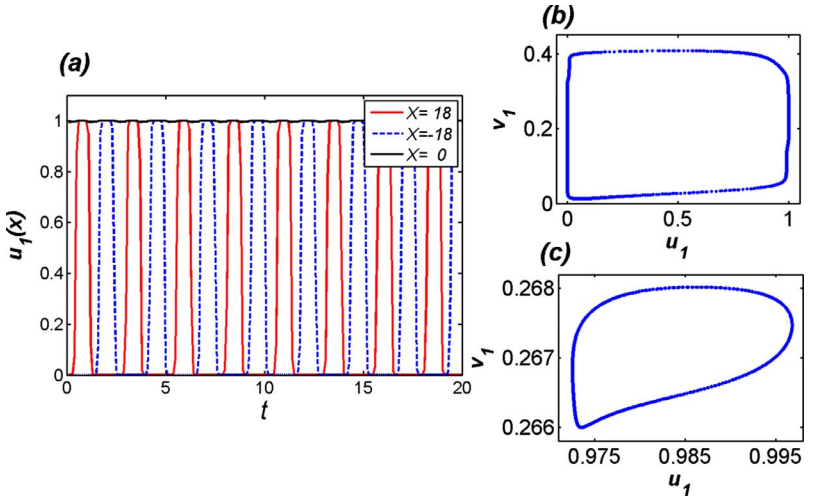

FIG. 4. (Color online) (a) The concentration of u_1 at the three points $X=18$ (solid red line), $X=-18$ (blue dashed line), and $X=0$ (solid black line) as a function of time t. (b) The u_1-v_1 cycle orbit at point $X=-18$. (c) The u_1-v_1 cycle orbit at point $X=0$.

C. Linear stability analysis and numeric analysis

The fixed point $(u_{1g},v_{1g},u_{2g},v_{2g})$ of coupled model (1)–(4) occurs when Eqs. (5)–(8) all equal 0 (neglecting the diffusion terms),

$$\frac{du_1}{dt} = \frac{1}{\varepsilon}u_{1g}(1-u_{1g})[u_{1g}-(v_{1g}+b)/a], \tag{5}$$

$$\frac{dv_1}{dt} = u_{1g}-v_{1g}-Kv_{1g}v_{2g}, \tag{6}$$

$$\frac{du_2}{dt} = \frac{1}{\varepsilon}u_{2g}(1-u_{2g})[u_{2g}-(v_{2g}+b)/a], \tag{7}$$

$$\frac{dv_2}{dt} = u_{2g}-v_{2g}-Kv_{1g}v_{2g}. \tag{8}$$

There are five solutions: A: $(u_{1g}=0,v_{1g}=0,u_{2g}=0,v_{2g}=0)$, B: $(u_{1g}=1,v_{1g}=1,u_{2g}=0,v_{2g}=0)$, C: $(u_{1g}=0,v_{1g}=0,u_{2g}=1,v_{2g}=1)$, D: $(u_{1g}=(v_{1g}+b)/a,u_{1g}=v_{1g}+Kv_{1g}v_{2g},u_{2g}=(v_{2g}+b)/a,v_{2g}=v_{1g},)$, and E: $(u_{1g}=1,v_{1g}+Kv_{1g}v_{2g}=1,u_{2g}=1,v_{2g}=v_{1g})$. Solution A is a stable fixed point for both the coupled model and the single model in Ref. [2]. Solutions B, C, and D are unstable because small perturbations of u_{1g} or u_{2g} will make u_1 or u_2 rapidly move away from that fixed point. Solution E maybe stable. We will discuss solution E in more detail below.

First, though, let us focus on the contacting point $(X=0)$. Because of the symmetry of the $u_{1,2}$ and $v_{1,2}$ pulses at this point, u_1 always equals u_2 and v_1 always equals v_2 at $X=0$. Then Eqs. (5)–(8) can be rewritten as

$$\frac{du}{dt} = \frac{1}{\varepsilon}u(1-u)[u-(v+b)/a], \tag{9}$$

$$\frac{dv}{dt} = u-v-Kv^2. \tag{10}$$

The fixed point E of Eqs. (5)–(8) then becomes $[u=1\equiv u_E, v=(\sqrt{1+4K}-1)/2K\equiv v_E]$. Assuming small perturbations $\Delta u(t)$ and $\Delta v(t)$ are added to the solution

$$u(t) = u_E+\Delta u(t), \quad v(t) = v_E+\Delta v(t). \tag{11}$$

Inserting Eq. (11) into Eqs. (9) and (10) and linearizing the equations for small Δu and Δv, we obtain the variational equations for the perturbations

$$\frac{d\Delta u}{dt} = -\frac{1}{\varepsilon}u_E[u_E-(v_E+b)/a]\Delta u, \tag{12}$$

$$\frac{d\Delta v}{dt} = \Delta u-(1+2Kv_E)\Delta v. \tag{13}$$

Assuming Δu and Δv have the form of $\Delta u\sim u_0\exp(\lambda t)$ and $\Delta v\sim v_0\exp(\lambda t)$, and inserting them into Eqs. (12) and (13), we can obtain the following matrix equations:

$$\begin{pmatrix} -\frac{1}{\varepsilon}u_E[u_E-(v_E+b)/a]-\lambda & 0 \\ 1 & -(1+2Kv_E)-\lambda \end{pmatrix}\begin{pmatrix} u_0 \\ v_0 \end{pmatrix} = 0. \tag{14}$$

Hence the characteristic equation is $\{\frac{1}{\varepsilon}u_E[u_E-(v_E+b)/a]+\lambda\}[(1+2Kv_E)+\lambda]=0$ and then

$$\lambda = -\frac{1}{\varepsilon}u_E[u_E-(v_E+b)/a], \quad \lambda = -(1+2Kv_E). \tag{15}$$

If $K>0$, $v_E=(\sqrt{1+4K}-1)/2K>0$. Therefore, if u_E and v_E satisfy

$$u_E\equiv 1>(v_E+b)/a \Rightarrow v_E<a-b, \tag{16}$$

λ will have negative values, and (u_E,v_E) is stable.

For $K=10$, $u_E=1$, and we can get $v_E\approx 0.27$, which is the value we observed in Fig. 4(c). So, the coupled system stays in this stable state at the contacting point. This is why $u_{1,2}$ values are always very high at the contact point. Taking advantage of the diffusion term, they can excite the surrounding media, on the side where the corresponding v_1 (or v_2) is lower, to generate new pulses that travel in the opposite direction from the former pulses.

As discussed earlier, for very small K values, $v_E=(\sqrt{1+4K}-1)/2K>a-b\approx 0.4$. The coupled system cannot reach the (u_E,v_E) state, for when $v_{1,2}>a-b$, $u_{1,2}$ will rapidly be decreased to 0, pushing $u_{1,2}$ and $v_{1,2}$ back to the (0,0) state. In this case, the coupled system generates pattern I, which mainly shows the properties of the single model in Ref. [2]. For proper larger K values satisfying $K>[1-(a-b)]/(a-b)^2$, which equals

$$v_E=(\sqrt{1+4K}-1)/2K<a-b, \tag{17}$$

the coupled system can easily reach the (u_E,v_E) state around the contacting region. However, if the value of v_E is close to the value of $(a-b)$, because v_1 and v_2 have different values outside the contacting region [see Fig. 3(b)–3(f)], and because Kv_1v_2 is much smaller when either v_1 or v_2 is very small, the larger one of $v_{1,2}$ can easily increase to a value larger than $(a-b)$. This pushes the corresponding $u-v$ back to the (0,0) state. The points then can reach the (u_E,v_E) state are now restricted in a limited domain around the contacting point, and they can have only small fluctuations due to the diffusion of $u_{1,2}$. The points outside this domain show the dynamic orbit in Fig. 4(b), which is the typical orbit in Ref. [2]. With these K values, pattern II appears.

For very large K values, Kv_1v_2 plays the main role in the coupled system. Also v_E is so small that the (u_E,v_E) state is very easy to reach. Then the domain that fills up with points in the (u_E,v_E) state expands, and pattern III appears.

We have plotted the numerically calculated phase diagrams of the $a-K$ plane and the $b-K$ plane in Figs. 5(a) and 5(b), respectively. When parameters locate in the region under the line $K=K_{\min}$, pattern I appears. When parameters locate in the region between the line $K=K_{\min}$ and the line $K=K_{\max}$, pattern II appears. When parameters locate in the region above the line $K=K_{\max}$, the coupled system generates pattern III. $K^*_{\min}$ is the minimum value determined by Eq. (17), and $K^*_{\min}=[1-(a-b)]/(a-b)^2$. We find that $K^*_{\min}$ lines have a similar shape to the corresponding $K_{\min}$ lines in both

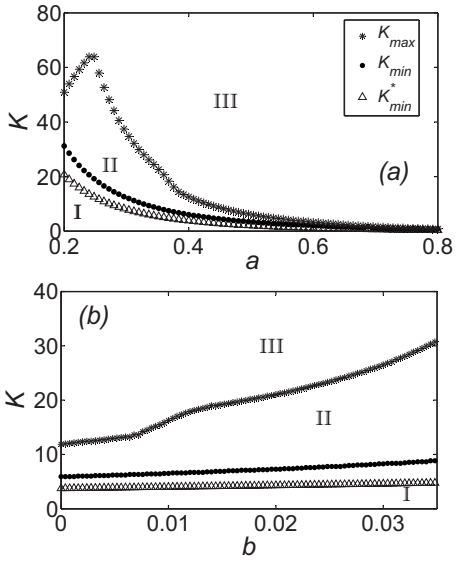

FIG. 5. (a) Phase diagram in the $a-K$ plane. Parameter b is fixed to be 0.003. (b) Phase diagram in the $b-K$ plane. Parameter a is fixed to be 0.4. Pattern I appears in the region where $K<K_{\min}$. Pattern II appears in the region where $K_{\min}<K<K_{\max}$. Pattern III appears in the region where $K>K_{\max}$. $K^*_{\min}$ is the analytical result from Eq. (17).

Figs. 5(a) and 5(b). That the computed $K_{\min}$ values are a little larger than $K^*_{\min}$ indicates that the v_E cannot be very close to $(a-b)$ if the (u_E,v_E) state is to be reached in the coupled system.

We have calculated the periodicity of the system to determine the effects of K. The inset of Fig. 6 shows, when $K=7$, for example, the time length between two following u_1 wave pulses approaching the same space point in the system. Horizontal coordinate N represents the Nth wave pulses of the wave train approaching this space point, beginning when two u_1 and u_2 pulses first contact each other. Vertical ordinate T represents the time length between the Nth and $(N+1)$th wave pulses approaching this space point. In this inset, we find that after a decreasing (adapting) process, the

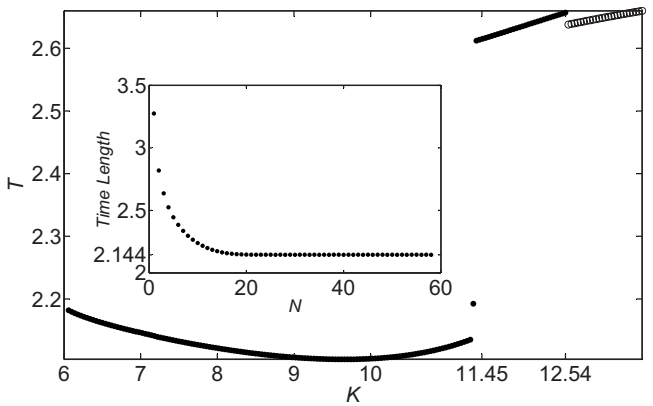

FIG. 6. The model's periodicity T vs parameter K. ○ represents oscillations that show pattern III. The inset shows, when $K=7$, for example, the time length between two following u_1 wave pulses approaching the same space point in the system after the initial stimulation.

time length between two neighboring wave pulses finally settles at a fixed value, which is the system's periodicity T. We show T vs K in Fig. 6. We find that for $K<6.06$, the two traveling waves cross each other without generating oscillations in their contacting regions (pattern I). For $K>12.55$, pattern III appears, and all the points in the simulation region eventually reach the state of (u_E,v_E) at last. For $6.06\leq K\leq 12.54$ there are stable oscillations generated in the contacting region (pattern II). The curve for $12.55<K\leq 13.44$ in Fig. 6 is shown to illuminate the difference between the pattern II and pattern III. As described in the former section, when the value of K is in this range, the system can generate wave trains but the domain around the contacting point which reach the (u_E,v_E) state expands. Because of this expanding domain, the periodicity T has a smaller value than when $K=12.55$. This explains the small drop in the curve at the point $K=12.55$ in Fig. 6. The periodicity T, when $12.55<K\leq 13.44$, is measured before the expanding domain reaches the fixed space point that is used to compute the number of wave trains.

As shown in Figs. 1 and 3, all of the four variables $u_{1,2}$ and $v_{1,2}$ are nonzero in the contacting region. As K increases, v_1 reacts with v_2 at a larger rate. For relatively large values of K, this reaction effectively weakens the inhibition effect of the inhibitors (v_1 and v_2) to their corresponding activators (u_1 and u_2). The regrowing velocity of the u_1 and u_2 waves increases, resulting in a decrease in periodicity (see Fig. 6 for $6.06\leq K<10.26$). However, for large enough values of K, v_1, and v_2 react with each other so quickly that one is annihilated before either variable can obviously affect the regrowing of u_1 or u_2. This results in an increase in T as K increases (see Fig. 6 for $10.26\leq K<12.55$). Eventually, around $K=11.36$, the periodicity T has an abrupt jump in value. We have no analytical explanation for this jump point as yet.

D. Dynamics when the two coupled models are different

It is very difficult to find two systems with the same dynamic constant, so we need to consider the differences of the two coupled reaction-diffusion systems. In our simulation, we found that if $b_1\neq b_2$, $D_1\neq D_2$, or $\varepsilon_1\neq\varepsilon_2$, then the u_1 and u_2 waves have different speeds of propagation. Because the speeds of these two kinds of activator pulses are different, as the pulses eventually travel a sufficiently long distance, the u_1 (or u_2) periodic waves are caught by the trailing u_2 (or u_1) waves. The regions of their coincidence act as new sources for generating periodic waves, making the system's oscillation behaviors very confused.

However, in this situation, the system's periodic behavior is size limited, as is also the case in the nature. The finite volume of natural systems ensures that this two-system coupled system can generate persistent periodic waves—the only essential condition is that before the waves reach the edges of these systems, they should not catch each other. In Fig. 7(a), we fix $a_1=a_2$, $\varepsilon_1=\varepsilon_2$, and $D_1=D_2$, and vary only b_2 to measure the relationship between the system's length L and the maximum difference Δb ($\Delta b=b_2-b_1$) that allows the system to generate persistent periodic waves. In the same

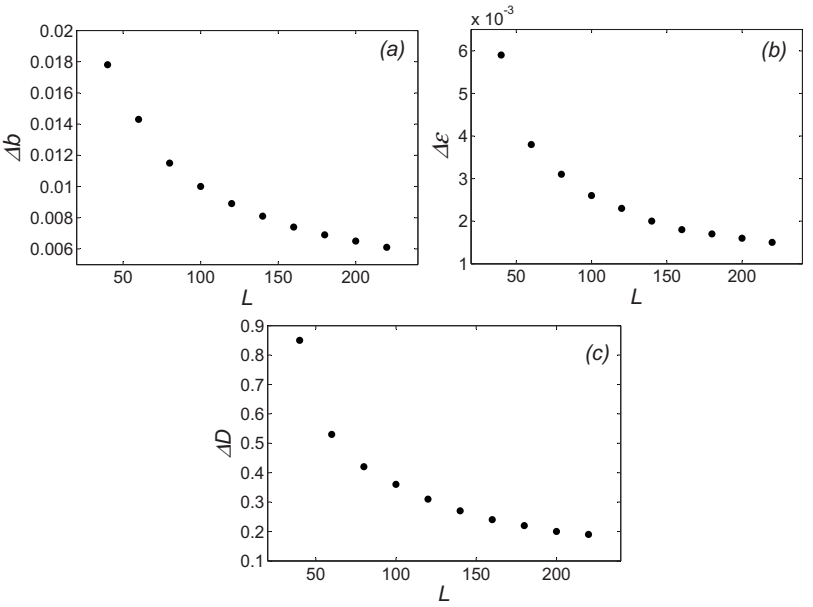

FIG. 7. (a) The relationship between the system's length L and the maximum difference Δb ($\Delta b = b_2 - b_1$) that can generate pattern II. The parameters are $K=10$, $a_1=a_2=0.4$, $b_1=0.003$, $\varepsilon_1=\varepsilon_2=0.0085$, and $D_1=D_2=1$. (b) The relationship between the system's length L and the maximum difference $\Delta\varepsilon$ ($\Delta\varepsilon=\varepsilon_2-\varepsilon_1$) that can generate pattern II. The parameters are the same as in (a), but also with $b_1=b_2=0.003$ and $\varepsilon_1=0.0085$. (c) The relationship between the system's length L and the maximum difference ΔD ($\Delta D=D_2-D_1$) that can generate pattern II. The parameters are the same as in (a) but also with $D_1=1$.

way, we fix other parameters and vary only ε_2 or D_2 to calculate the relationship between L and the maximum difference $\Delta\varepsilon$ and ΔD, respectively. These results are plotted in Figs. 7(b) and 7(c). From Fig. 7, we see that as the simulated system's length is increased, the two coupled systems must be similar to ensure the generation of persistent periodic waves.

The difference of parameters a_1 and a_2 causes another problem in the coupled system. If $a_1 \neq a_2$, then the frequencies of generating new u_1 and u_2 pulses in the contacting region are different. After a sufficient time, u_1 and u_2 waves are generated in the same place and move in the same direction. Then, they contact each other outside the former contacting region. As the new contact region generates other $u_{1,2}$ pulses, the periodic behaviors of the whole system are destroyed. To prolong the time of the system's periodic behavior, the maximum difference Δa ($\Delta a = a_2 - a_1$), which can generate periodic waves in a limited time, should be decreased.

We also find that differences in a_1 and a_2 greatly affect the minimum and maximum values of K that can generate periodic waves. In Fig. 8, we fix other parameters, and then plot the relationship between Δa and $K_{\min}$, and Δa and $K_{\max}$ in a fixed observation time $t=20$. In this time, beginning at the first contact of the u_1 and u_2 pulses, the system can generate periodic wave trains with K in the range of $K_{\min} \leq K \leq K_{\max}$. We see that changes to Δa cause great changes to the difference between $K_{\min}$ and $K_{\max}$ [in contrast with Fig. 5(a), for example]. In our simulations, we also find that if a_2 is larger (smaller) than a_1, then the system's oscillation time can be prolonged by increasing (decreasing) D_2 or decreasing (increasing) ε_2. This provides a means of selecting two similar reaction-diffusion systems if one wants to couple them and achieve stable oscillation conditions.

E. Two-dimensional patterns

In two-dimensional systems (where $\nabla^2 = \partial^2/\partial X^2 + \partial^2/\partial Y^2$), the coupled model can generate many more complex and interesting patterns. In Figs. 9 and 10, we show two different pattern evolutions for two different initial conditions. In Fig. 9, the four points grow as four target waves before they meet each other. When two u_1 (or two u_2) activator waves contact each other, the waves vanish because they are followed by two v_1 (or two v_2) inhibitor waves. When the two activator waves are u_1 and u_2 waves, the waves begin to oscillate in their contacting regions, to generate periodic waves and create complex patterns, as shown in Fig. 9. In Fig. 10, the initial condition leads to yet another complex pattern. All six subgraphs of these two figures have a time interval of 20. The patterns generated by our 2D coupled system are more complex because the initial patterns have their own shapes. They have different contact times in different contact regions. These interesting patterns are created by their different oscillation behaviors.

III. GENERALITY OF THIS COUPLING EFFECT

A. Coupled catalytic CO oxidation on Pt(110) model

To check whether this coupling effect is model dependent, we apply our method to the models for catalytic CO oxida-

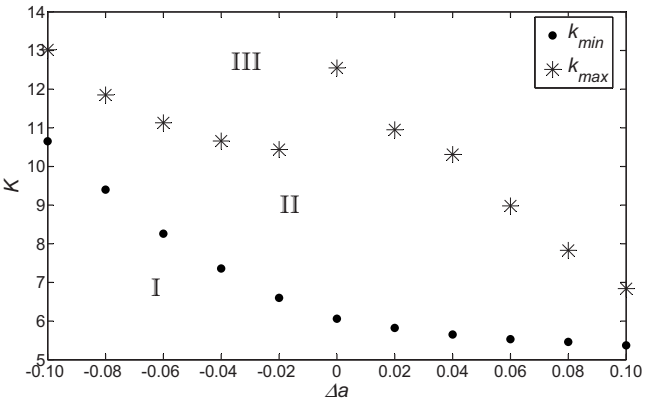

FIG. 8. The relationship between Δa and $K_{\min}$, and Δa and $K_{\max}$ that can generate periodic waves in a fixed observation time $t=20$. The other parameters are fixed.

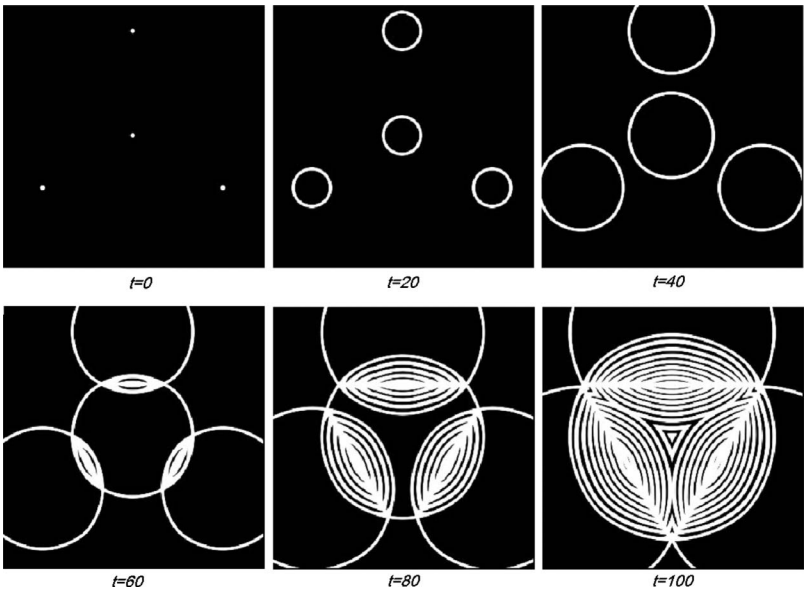

FIG. 9. The spatiotemporal evolution from the initial condition subgraph $t=0$ (For the middle point, u_1 is nonzero. For the three surrounding points, u_2 is nonzero).

tion on Pt(110) [26–29] and cardiac tissue [30,31]. The coupled catalytic CO oxidation on Pt(110) model we used is

$$\frac{\partial u_1}{\partial t} = \frac{1}{\varepsilon} u_1(1-u_1)[u_1 - (v_1+b)/a] + D\nabla^2 u_1, \tag{18}$$

$$\frac{\partial v_1}{\partial t} = f(u_1) - v_1 - Kv_1v_2, \tag{19}$$

$$\frac{\partial u_2}{\partial t} = \frac{1}{\varepsilon} u_2(1-u_2)[u_2 - (v_2+b)/a] + D\nabla^2 u_2, \tag{20}$$

$$\frac{\partial v_2}{\partial t} = f(u_2) - v_2 - Kv_1v_2, \tag{21}$$

where $f(u)=0$ if $0 \le u < 1/3$; $f(u)=1-6.75u(u-1)^2$ if $1/3 \le u \le 1$; and $f(u)=1$ if $u>1$. Using the parameters in [26–29], we get the phase diagram in the $K-a$ and $K-b$ planes, shown in Figs. 11(a) and 11(b) respectively, and we show which parameter values lead to the generation of patterns I, II, and III.

We also compute the relationship between K and the system's periodicity T. This result is plotted in Fig. 12(a). Because the value of a in [26–29] is 0.84, much larger than that in our former Barkley-type model in which $a=0.4$, the range of parameter K that can generate steady oscillation waves is more narrow [as predicted in Fig. 5(a)]. We show, in Figs. 11 and 12(a), that the oscillation behavior also exists in the model for catalytic CO oxidation on Pt(110). Considering that the main difference between this and the Barkley-type model is the function $f(u)$, we use the parameter values of the Barkley-type model with this model in Fig. 12(b) to plot the curve $T(K)$. It is because of the function $f(u)$ that Fig. 12(b) differs from Fig. 6. The range of K that can generate steady wave trains is a little smaller than that in Fig. 6, and

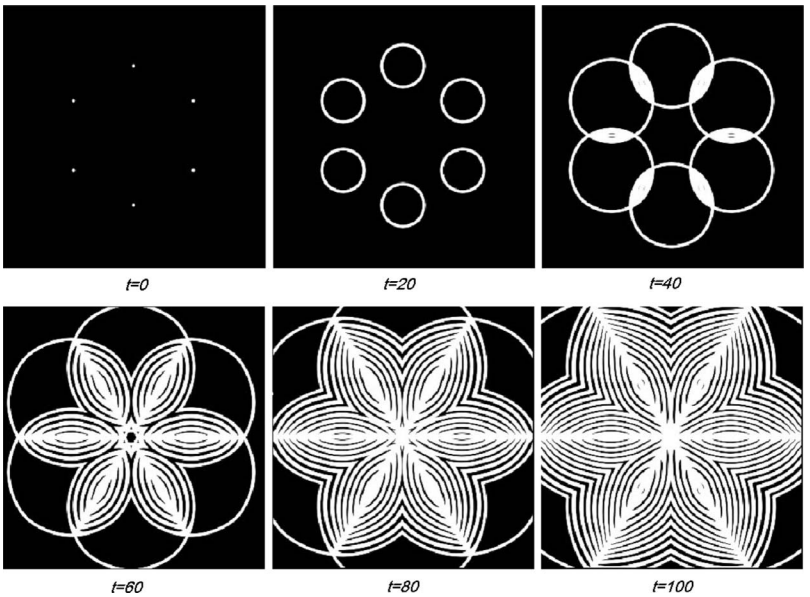

FIG. 10. The spatiotemporal evolution from the initial condition subgraph $t=0$ (Clockwise from the top, for the first, third, and fifth points, u_1 is nonzero. For the other three points, u_2 is nonzero).

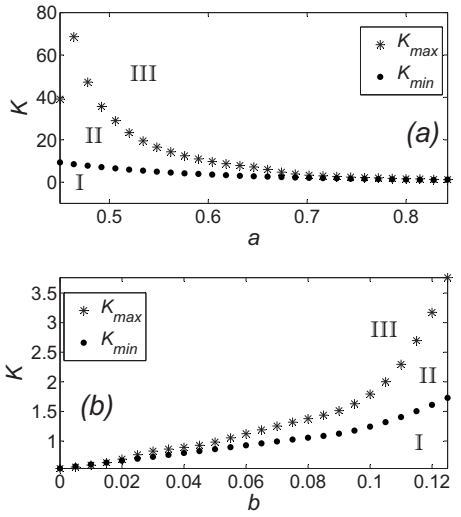

FIG. 11. Phase diagrams of the catalytic CO oxidation on Pt(110) model. (a) Phase diagram in the $a-K$ plane. Parameters are $\varepsilon=0.01$, $D=1$, with b fixed to be 0.07. (b) Phase diagram in the $b-K$ plane. Parameter a is fixed to be 0.84.

so is the range of the periodicity T. The main shape of these two figures is the same, though, and they follow almost the same dynamic behaviors.

B. Coupled cardiac tissue model

We couple the cardiac tissue model as follows:

$$\frac{\partial e_1}{\partial t} = \nabla^2 e_1 - p_0[f(e_1) + g_1], \tag{22}$$

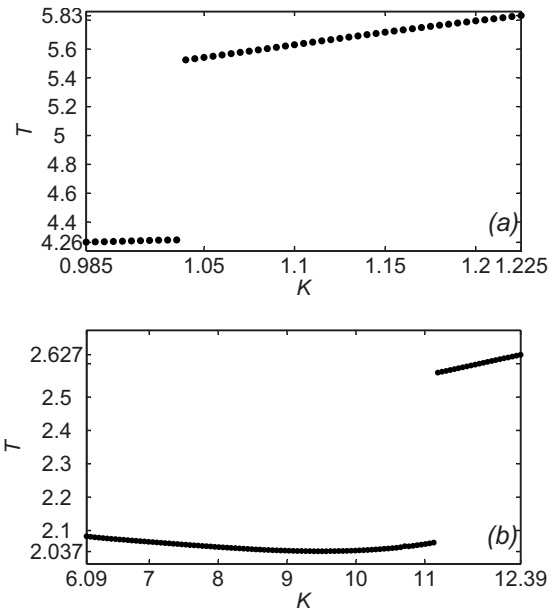

FIG. 12. The periodicity T vs K of the model for catalytic CO oxidation on Pt(110). (a) Parameters are $a=0.84$, $b=0.07$, $\varepsilon=0.01$, and $D=1$, as in Refs. [26–29]. (b) Parameters are $a=0.4$, $b=0.003$, $\varepsilon=0.0085$, and $D=1$, as in Ref. [2].

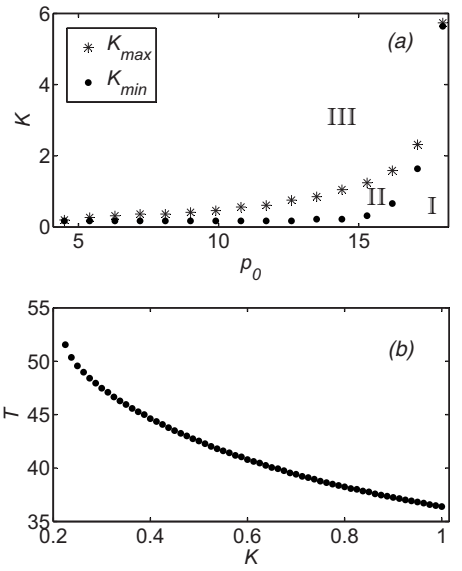

FIG. 13. (a) Phase diagram in the p_0-K plane of the model for cardiac tissue. (b) The periodicity T vs K of the model for cardiac tissue. In both (a) and (b), the parameters are $e_a=0.0026$, $e_b=0.837$, $C_1=20$, $C_2=3$, $C_3=15$, $a=0.06$, $p=3$, $g_a=1.8$, $\varepsilon_a=1/75$, $\varepsilon_b=1.0$, and $\varepsilon_c=0.3$ as in Refs. [30,31]. Additionally, in (b), $p_0=15$.

$$\frac{\partial g_1}{\partial t} = \varepsilon(e_1, g_1)(pe_1 - g_1 - Kg_1g_2), \tag{23}$$

$$\frac{\partial e_2}{\partial t} = \nabla^2 e_2 - p_0[f(e_2) + g_2], \tag{24}$$

$$\frac{\partial g_2}{\partial t} = \varepsilon(e_2, g_2)(pe_2 - g_2 - Kg_1g_2), \tag{25}$$

where $f(e)=C_1e$ when $e<e_a$; $f(e)=-C_2e+a$ when $e_a\leq e\leq e_b$; $f(e)=C_3(e-1)$ when $e>e_b$, and $\varepsilon(e,g)=\varepsilon_a$ when $e<e_b$; $\varepsilon(e,g)=\varepsilon_b$ when $e>e_b$; $\varepsilon(e,g)=\varepsilon_c$ when $e<e_a$ and $g<g_a$. If $p_0=1$, then the whole system is the same as that in [30,31]. However, we find that the system cannot generate pattern II until $p_0\gg 1$ (for $K\approx 0.4$, it can generate pattern III). In other words, the reaction velocity of the activators should be much larger than the inhibitors'. Then, the excitable system can generate steady oscillations. In Fig. 13(a) we show the phase diagram in the p_0-K plane. Pattern II appears in a narrow region. When $p_0=15$, for example, the relationship between coupling constant K and the system's periodicity T is shown in Fig. 13(b). We find that for $0.21\leq K\leq 1$ the system can generate steady wave trains, and that the periodicity T is much larger than in models (1)–(4) and (18)–(21). Unlike the former two models, the $T(K)$ is a continuous function with no jump points. Significantly, both of models (18)–(25) exhibit the coupling effect. Both models also demonstrate the universality of a spontaneous wave generator in excitable media.

IV. CONCLUSION AND DISCUSSION

In this paper, we propose a coupled reaction-diffusion model based on the general model in excitable media. In the region where two coupled traveling waves make contact, a wave generator is observed that produces periodic wave trains that need no external force after the initial stimulation. Complex two-dimensional patterns are found in the simulation. We discuss the influence of the coupling constant, the systems' parameters, and the influence of the two systems' different dynamic constants on the dynamic behavior of the coupled system. We measure the maximum differences of each key parameter for finite system sizes or finite reaction times. Also, we observe that this coupling effect is not model dependent. It is found in the model for catalytic CO oxidation on Pt(110), as well as in the cardiac tissue model. As shown by phenomena from the three models in our paper, this coupling effect can be verified by finding two similar activator-inhibitor systems in which the two inhibitors can react with each other and vanish at a proper reaction velocity. Since excitability is ubiquitous in all areas of science, we hope our work will contribute to the exploration of more complex patterns in nature.

ACKNOWLEDGMENTS

We are grateful to John Eliades and Jianxin Bao for helpful suggestions. We thank Kathy Watts for the help in the English improvement of this paper. We also thank Shumin Zhao, Minggang Xia, and Erhu Zhang for valuable discussions. This work was supported by NSF of China under Grant No. 10374075, and the Keygrant Project of Chinese Ministry of Education under Grant No. 708082.

[1] J. D. Murray, *Mathematical Biology*, 2nd ed. (Springer, New York, 1993).
[2] D. Barkley, M. Kness, and L. S. Tuckerman, Phys. Rev. A **42**, 2489 (1990).
[3] A. T. Winfree, Science **175**, 634 (1972).
[4] V. K. Vanag, L. Yang, M. Dolnik, A. M. Zhabotinsky, and I. R. Epstein, Nature (London) **406**, 389 (2000).
[5] K. Agladze, J. P. Keener, S. C. Müller, and A. Panfilov, Science **264**, 1746 (1994).
[6] I. Schebesch and H. Engel, Phys. Rev. E **57**, 3905 (1998).
[7] K. J. Lee, E. C. Cox, and R. E. Goldstein, Phys. Rev. Lett. **76**, 1174 (1996).
[8] J. M. Davidenko, A. V. Pertsov, R. Salomonsz, W. Baxter, and J. Jalife, Nature (London) **355**, 349 (1992).
[9] A. Karma, Phys. Rev. Lett. **71**, 1103 (1993).
[10] S. Zhang, B. Hu, and H. Zhang, Phys. Rev. E **67**, 016214 (2003).
[11] H. Zhang, B. Hu, and G. Hu, Phys. Rev. E **68**, 026134 (2003).
[12] M. Perc, Phys. Rev. E **72**, 016207 (2005).
[13] H. Wang, K. Zhang, and Q. Ouyang, Phys. Rev. E **74**, 036210 (2006).
[14] O. Steinbock, V. S. Zykov, and S. C. Müller, Nature (London) **366**, 322 (1993).
[15] V. Petrov, Q. Ouyang, and H. L. Swinney, Nature (London) **388**, 655 (1997).
[16] I. Sendina-Nadal, E. Mihaliuk, J. Wang, V. Perez-Munuzuri, and K. Showalter, Phys. Rev. Lett. **86**, 1646 (2001).
[17] S. Naknaimueang, M. A. Allen, and S. C. Müller, Phys. Rev. E **74**, 066209 (2006).
[18] S. Grill, V. S. Zykov, and S. C. Müller, Phys. Rev. Lett. **75**, 3368 (1995).
[19] M. Hildebrand, H. Skodt, and K. Showalter, Phys. Rev. Lett. **87**, 088303 (2001).
[20] V. K. Vanag, L. Yang, M. Dolnik, A. M. Zhabotinsky, and I. R. Epstein, Nature (London) **406**, 389 (2000).
[21] M. Hildebrand, J. Cui, E. Mihaliuk, J. Wang, and K. Showalter, Phys. Rev. E **68**, 026205 (2003).
[22] Q. Li and X. Lang, Phys. Rev. E **74**, 031905 (2006).
[23] R. Karnatak, R. Ramaswamy, and A. Prasad, Phys. Rev. E **76**, 035201(R) (2007).
[24] D. M. Petrich and R. E. Goldstein, Phys. Rev. Lett. **72**, 1120 (1994).
[25] T. Ohta, Y. Hayase, and R. Kobayashi, Phys. Rev. E **54**, 6074 (1996).
[26] M. Bär and M. Eiswirth, Phys. Rev. E **48**, R1635 (1993).
[27] M. Hildebrand, M. Bär, and M. Eiswirth, Phys. Rev. Lett. **75**, 1503 (1995).
[28] J. Yang, F. Xie, Z. Qu, and A. Garfinkel, Phys. Rev. Lett. **91**, 148302 (2003).
[29] C. Zemlin, K. Mukund, M. Wellner, R. Zaritsky, and Arkady Pertsov, Phys. Rev. Lett. **95**, 098302 (2005).
[30] A. V. Panfilov and P. Hogeweg, Phys. Lett. A **176**, 295 (1993).
[31] S. Sinha, A. Pande, and R. Pandit, Phys. Rev. Lett. **86**, 3678 (2001).